SIAM J. CONTROL OPTIM.
Vol. 56, No. 1, pp. 556–581

ELASTO-PLASTIC SHAPE OPTIMIZATION USING THE LEVEL SET METHOD*

AYMERIC MAURY†, GRÉGOIRE ALLAIRE‡, AND FRANÇOIS JOUVE§

Abstract. This article is concerned with shape optimization of structures made of a material obeying Hencky's laws of plasticity, with the stress bound expressed by the von Mises effective stress. The ill-posedness of the model is circumvented by using two regularized versions of the mechanical problem. The first one is the classical Perzyna formulation which is regularized, and the second one is a new regularized formulation proposed for the von Mises criterion. Shape gradients are calculated thanks to the adjoint method. The optimal shape is numerically computed by using the level set method. To illustrate the validity of the method, 2D examples are performed.

Key words. topology and shape optimization, perfect plasticity, Hencky model, level set method, penalization, regularization

AMS subject classifications. 35J60, 35J88, 49Q10, 49Q12, 74C05, 74C10, 74P05, 74P10, 74P15

DOI. 10.1137/17M1128940

1. Introduction.

As shape optimization becomes more and more popular in industrial applications, the ability to take into account nonlinear mechanical behaviors is of great need. Plasticity ones are some of the most used since the associated models account for irreversible microscopic mechanical defects. These defects result in plastic areas which tend to deform more than elastic ones. This may lead to weak structural integrity and breaking. In this case, the designer often tries to avoid the creation of plastic regions by controlling the internal constraints. But plasticity may also be useful when, for instance, the breaking of a piece is meant to protect other parts which are difficult to repair or which should absolutely not collapse (such as in the use of circuit breakers in electricity). There exist materials, called ductile, which can suffer significant deformations after the elastic phase (without collapsing), and the designer can take advantage of this property by allowing plastic areas and trying to distribute the constraint throughout the structure in the most uniform way possible.

From a mechanical point of view, plasticity was first studied by Tresca, Saint Venant, Lévy, and Bauschinger in the 19th century and by Prandtl, von Mises, and Reuss in the 20th century. From a mathematical point of view, the study was initiated by Prager, Drucker, and Hill and continued by Moreau [45] and Duvaut and Lions [14] using the theory of variational inequalities and convex analysis. Since then, many articles have been published on the subject, investigating the well-posedness of these problems. We particularly mention Suquet [64], Temam [67], and the more recent

*Received by the editors May 5, 2017; accepted for publication (in revised form) December 5, 2017; published electronically February 22, 2018. The first author conducted most of the work related to this article while at Laboratoire J.L. Lions (UMR CNRS 7598), University Paris Diderot, Paris, France. The second author is a member of the DEFI project at INRIA Saclay Ile-de-France.
http://www.siam.org/journals/sicon/56-1/M112894.html
Funding: This work was supported by the RODIN project (FUI AAP 13).
†GIREF, Département de mathématiques et de statistique, Université Laval, Québec G1V 0A6, Canada (amaury@cmap.polytechnique.fr).
‡CMAP, Ecole Polytechnique, CNRS, Université Paris-Saclay, 91128 Palaiseau, France (gregoire.allaire@polytechnique.fr).
§Laboratoire J.L. Lions (UMR CNRS 7598), University Paris Diderot, Paris, France (jouve@ljll.univ-paris-diderot.fr).

papers of Dal Maso and coworkers [8], [9]. Concerning the regularity of solutions, the reader is referred to [16] and [4].

This article focuses on shape optimization with the level set method for static perfect plasticity, also called the Hencky model, for the von Mises criterion (also called the Huber–Mises or Huber–Mises–Hencky criterion). As pointed out in [64], the Hencky plasticity is not mechanically relevant except in some very specific cases. It does not account for the path dependency shown by the experiments and thus is rather a nonquadratic law. However, it raises a great amount of the mathematical difficulties of the quasi-static case. Moreover, when the numerical solution of the quasi-static evolution comes into question, a time discretization leads to a sequence of the Hencky model which needs to be solved. Finally, for the shape optimization it will be easier to first study this steady problem, as time-dependent problems lead to backward adjoint problems.

The problem can be put into a mixed form including a variational inequality and a variational equation. Due to the appearance of a variational inequality, there is no chance for this problem to be Fréchet or Gateaux differentiable. The solution we choose, which was largely investigated in the framework of control theory for problems with hardening but not in the framework of shape optimization, involves the use of a regularized penalized problem to get rid of the variational inequality. We refer the reader, for the static case, to [24], [26], [27], [11] (using a primal formulation) and [28], [5] (for a second-order optimality condition), to [69] for the quasi-static case, and to [10] and [36] for other plastic models.

In shape optimization, the first case which was considered was that of beam structure and frame optimization, which is addressed, for instance, in [33], [17], [66], [32], [1], [50], [35]. We point out the particular case of [74], where periodical microstructures are used. From a theoretical point of view, in [62, Chapter 4.8], the shape derivative of an elasto-plastic torsion problem is computed, and in [62, Chapter 4.9] the shape derivative of the stress tensor is calculated in the case of the visco-plastic model of Perzyna (see section 3). There also exist numerous articles in which, for a particular optimization problem, the existence of a solution is proved for the continuous and discrete cases, assuming a uniform Lipschitz boundary. The discrete solution is then proved to converge to the continuous case. In [29] (see also [21] and [22]), the analysis is done in the framework of the Hencky model for a criterion depending only on σ. In [31], the analysis is done for axisymmetric bodies. In [30], the same analysis is done in the case of the Prandtl–Reuss model of elasto-plasticity (dynamic plasticity). In [52] strain-hardening is added. Finally, [13] and [20] (for numerical results) deal with a particular elasto-plasticity model (introduced by Washizu in [71]).

From a numerical point of view, some authors use conical derivatives inside a bundle algorithm to optimize the shape; see [54] and [39]. Another way to proceed is to differentiate the radial return algorithm (the generalized Newton method; see [56, Chapter 8]). The differentiation is analyzed in [68], [40], and [44]. This procedure was applied in various articles using the von Mises criterion. In [43] and [57], the authors consider linear isotropic hardening/softening. They use, first, the solid isotropic material with penalization (SIMP) method and finish the shape optimization using splines to parameterize the boundary and recover smooth shapes. In [37], rate-independent elasto-plasticity and contact friction are taken into account. For the shape optimization, splines are used. In [38], the same is done but for finite deformation elasto-plasticity. In [34], the elasto-plastic model is the same but the derivative is computed differently. It also performs two-phase optimization by using the SIMP method. For perfect plasticity we mention [15], using the boundary pertur-

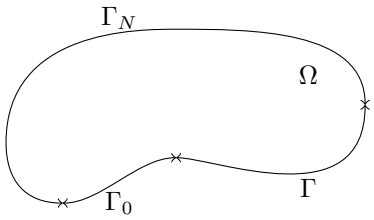

FIG. 1. *The open set* Ω.

bation method. We also mention that, based on the two regularized plasticity models presented here, we manage to extend our approach to quasi-static perfectly plastic problems.

Section 2 describes perfect plasticity from both a mechanical and a mathematical point of view, introducing the formulations and spaces classically used to study this particular behavior. Section 3 focuses on two ways to regularize the Hencky model. The first is the well-known Perzyna formulation, and the second is a new regularization adapted to the von Mises criterion. For each of them we give theorems proving existence and uniqueness of solutions as well as the convergence of the regularized solutions to the solution of static perfect plasticity. In section 4, a general shape optimization is introduced, and shape gradients are computed by virtue of the adjoint method. Section 5 recalls the basis of the level set method and briefly describes how the plasticity problems are numerically solved. Finally, our numerical results, performed with the freely available Scilab software [58], are gathered in section 6.

2. Elasticity and perfect plasticity.

2.1. Mechanical model. In this paper, Ω denotes an open bounded subset of $\mathbb{R}^d$ (see, for instance, Figure 1), where $d = 2$ or 3 and represents the shape of the structure we want to optimize. Its boundary is divided into three disjoint parts, meaning that

$$\partial\Omega = \Gamma_0 \cup \Gamma_N \cup \Gamma.$$

On Γ_0, the structure is clamped, and on Γ_N a force is applied. The free part of the boundary is Γ. The structure Ω is filled with a linear isotropic perfect plastic material, with Hooke's law defined by a fourth-order tensor A such that, for any symmetric matrix τ,

$$A\tau = 2\mu\tau + \lambda Tr(\tau) I_d, \tag{1}$$

where μ and λ are the Lamé moduli.

We consider that the material follows the Hencky law [14] of plasticity, which is a finer description of the material behavior than linearized elasticity, from which it is derived. We recall that in linearized elasticity the stress tensor σ is linearly related to the strain $e(u) = \frac{1}{2}(\nabla u +^t \nabla u)$ by $\sigma = Ae(u)$. Plasticity is based on a decomposition of the strain tensor into two parts [19, Chapter 3]. The first is the elastic strain, denoted by e_e, and the second is the plastic strain, e_p. Then we have

$$e(u) = e_e + e_p. \tag{2}$$

It has to be mentioned that if $e(u)$ is the symmetric part of the gradient of the displacement u, it is not the case for e_e and e_p, which are, however, symmetric. The

stress tensor σ is only related to the elastic part,

$$\sigma = Ae_e, \tag{3}$$

and replacing it in (2) yields

$$e(u) = A^{-1}\sigma + e_p. \tag{4}$$

The other fundamental ingredients are the elastic region and the yield surface. When σ is, in a certain set, called the elastic region, the plastic strain is equal to zero, $e_p = 0$. When σ is on the yield surface, which is the boundary of the elastic region, the plastic strain can vary. In this article, these regions are defined by a continuous function $\mathcal{F}$, called the yield function. Thus we define K_M as a subset of symmetric second-order tensors,

$$K_M = \left\{\tau \in \mathbb{M}_s^d \text{ such that } \mathcal{F}(\tau) \leq 0\right\}, \tag{5}$$

with $\mathbb{M}_s^d$ the space of symmetric second-order tensors in dimension d. The elastic region corresponds to $\mathcal{F}(\tau) < 0$, and the yield surface is defined by $\mathcal{F}(\tau) = 0$. When the system is on the yield surface, we define the plastic strain e_p by assuming the maximal plastic work (or Hill) principle,

$$\sigma : e_p \geq \tau : e_p \quad \forall \tau \in K_M,$$

which implies that e_p belongs to the normal cone of K_M. This defines the flow rule of our model. The flow rule in plasticity defines the evolution of the plastic strain e_p with respect to σ. When the plastic strain rate is in the normal cone of K_M (as it is the case when the maximal plastic work principle is assumed), one talks about associated plasticity. If it is not the case, one talks about nonassociated plasticity. We can sum up the different equations which characterize the evolution of the perfect elasto-plastic material, assuming the Hill principle satisfied, as

$$\begin{cases} e(u) & = e_p + A^{-1}\sigma, & \\ e_p : (\tau - \sigma) & \leq 0 & \forall \tau \in K_M, \\ \sigma \in K_M & & \\ -\operatorname{div}(\sigma) & = f & \text{in } \Omega, \\ u & = 0 & \text{on } \Gamma_0, \\ \sigma n & = g & \text{on } \Gamma_N, \\ \sigma n & = 0 & \text{on } \Gamma. \end{cases} \tag{6}$$

The three first lines of (6) are pointwise relations in Ω. In Figure 2(a) we plot, for a 1D case, the Hencky law, and in Figure 2(b) the corresponding quasi-static law, which can be retrieved in the same way as that for the static case. In a 1D example, the elastic region is an interval $[-\sigma_c, \sigma_c]$. When the stress σ reaches the threshold value σ_c, the plastic strain, and consequently the whole strain, can increase without any growth of the stress.

2.2. Mathematical model. We first need to introduce some functional spaces

$$H_s(\operatorname{div}, \Omega) = \left\{\tau \in L^2(\Omega; \mathbb{M}_s^d) \,|\, \operatorname{div}\tau \in L^d(\Omega)^d\right\},$$

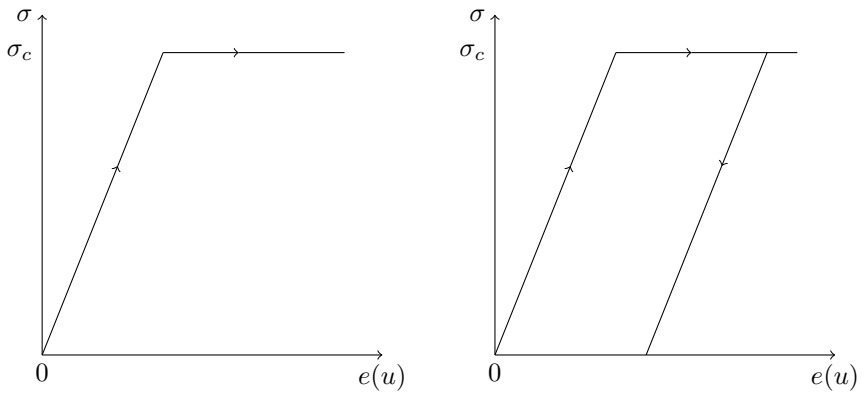

(a) Hencky's law. (b) Quasi-static law.

FIG. 2. *Hencky and quasi-static laws.*

where $\mathbb{M}^d_s$ is the space of symmetric second-order tensors in dimension d. This space is studied in [18] and [6]. The trace operator is not defined, but a normal trace operator γ_N can be defined as follows: to each $\tau \in H_s(\mathrm{div}, \Omega)$ it associates its normal trace $\tau n \in H^{-\frac{1}{2}}(\partial\Omega; \mathbb{R}^d)$. Then, for a given $g \in H^{-\frac{1}{2}}(\partial\Omega; \mathbb{R}^d)$, let

$$\Sigma_{\mathrm{div}}(g) = \{\tau \in H_s(\mathrm{div}, \Omega) \,|\, \gamma_N(\tau) = g\}\,.$$

The space of statically admissible stresses is defined by

$$S(f, g) = \{\tau \in \Sigma_{\mathrm{div}}(g) \,|\, -\mathrm{div}\tau = f \text{ in } \Omega\}\,.$$

Finally, introduce the convex set

$$K = \left\{\tau \in L^2(\Omega; \mathbb{M}^d_s) \,|\, \tau(x) \in K_M \text{ a.e. in } \Omega\right\},$$

where K_M is defined by (5), and the space of displacements

$$H^1_{\Gamma_0}(\Omega)^d = \left\{u \in H^1(\Omega)^d \text{ such that } u = 0 \text{ on } \Gamma_0\right\}.$$

Assume $\sigma \in S(f, g)$ and, at first, $u \in H^1_{\Gamma_0}(\Omega)^d$. In what follows, we give two different formulations of problem (6).

2.2.1. The dual problem. The first formulation is independent of u. It was established in [67] and produces a minimization problem solved by σ:

$$\sigma = \mathrm{argmin}_{\tau \in S(f,g)} \psi^*(\tau), \tag{7}$$

with $\psi^*(\sigma) = \frac{1}{2} A^{-1}\sigma : \sigma + \mathbb{1}_{K_M}(\sigma)$ and $\mathbb{1}_{K_M}$ the indicator function of K_M. The dual problem (7) can also be written in the form

$$\begin{cases} \max\limits_{\sigma \in K} -\dfrac{1}{2} \displaystyle\int_\Omega A^{-1}\sigma : \sigma \, dx \\ \text{under the constraint} \\ \displaystyle\int_\Omega \sigma : \epsilon(v)\, dx = \int_\Omega f \cdot v \, dx + \int_{\Gamma_N} g \cdot v \, ds \;\; \forall v \in H^1_{\Gamma_0}(\Omega)^d, \end{cases} \tag{8}$$

which admits a variational inequality formulation as follows: find $\sigma \in S(f,g) \cap K$ such that for every $\tau \in S(f,g) \cap K$,

$$\int_\Omega A^{-1}\sigma : (\tau - \sigma)\, dx \geq 0. \tag{9}$$

In [14, Chapter 5, section 6.3], the computations which enable us to pass from (6) to (9) (and consequently to (8)) are given (see also [67, Chapter 1, section 3.2]). Theorem 4.1 in [67] and Theorem 6.1 in [14] give the existence and uniqueness of a solution.

THEOREM 2.1. *If $S(f,g) \cap K \neq \emptyset$, problem* (8) *has a unique solution.*

2.2.2. The displacement problem. At first glance, it may seem that problem (6) can also be written under the following variational formulation coupling a variational inequality with a variational equation:

$$\begin{cases} \displaystyle\int_\Omega \sigma : e(v)\, dx = \int_\Omega f \cdot v\, dx + \int_{\Gamma_N} g \cdot v\, ds \ \ \forall v \in H^1_{\Gamma_0}(\Omega)^d, \\ \displaystyle\int_\Omega A^{-1}\sigma : (\tau - \sigma)\, dx \geq \int_\Omega e(u) : (\tau - \sigma)\, dx \ \ \forall \tau \in K. \end{cases} \tag{10}$$

Since the variational inequality in (10) is the characterization of the projection on K, with the norm associated with the scalar product of A^{-1}, denoting this projection by $P_K^{A^{-1}}$ implies that

$$\sigma = P_K^{A^{-1}}(Ae(u)), \tag{11}$$

and (10) is equivalent to

$$\int_\Omega P_K^{A^{-1}}(Ae(u)) : e(v)\, dx = \int_\Omega f \cdot v\, dx + \int_{\Gamma_N} g \cdot v\, ds \ \ \forall v \in H^1_{\Gamma_0}(\Omega)^d. \tag{12}$$

Unfortunately, it is not possible to prove the existence of a solution to (12) in the space $H^1_{\Gamma_0}(\Omega)^d$. On this subject, we refer the reader to [56, Chapter 2, section 3.6] or [72] for a mathematical explanation. Another way to understand this issue is to come back to the mechanical meaning of plasticity and the fact that it models dislocations in the material, which can produce displacement discontinuities through $(d-1)$-dimensional surfaces (see [64], [67, Chapter 6], and [46, Chapter V, section 3.4]). To circumvent this difficulty, a space of possibly discontinuous displacements was introduced in [63] and [67] that is the space of bounded deformation $BD(\Omega)$, which is similar to the space of bounded variation $BV(\Omega)$, and is defined by

$$BD(\Omega) = \left\{ u \in L^1(\Omega)^d \,|\, e(u) \in M_1(\Omega; \mathbb{M}^d_s) \right\},$$

with $M_1(\Omega; \mathbb{M}^d_s)$ being the space of bounded measures on Ω, with values in the space of $d \times d$ symmetric tensors. The correct formulation is then as follows: find $(\sigma, u) \in K \times BD(\Omega)$ such that

$$\begin{cases} \displaystyle\int_\Omega \sigma : e(v)\, dx = \int_\Omega f \cdot v\, dx + \int_{\Gamma_N} g \cdot v\, ds \ \ \forall v \in H^1_{\Gamma_0}(\Omega)^d, \\ \displaystyle\int_\Omega A^{-1}\sigma : (\tau - \sigma)\, dx \geq -_{L^{\frac{d}{d-1}}} \langle u, \operatorname{div}(\tau - \sigma) \rangle_{L^d} \ \ \forall \tau \in K \cap \Sigma_{\operatorname{div}}(g). \end{cases} \tag{13}$$

The brackets ${}_{L^{\frac{d}{d-1}}}\langle\,,\,\rangle_{L^d}$ denote the duality product between $L^{\frac{d}{d-1}}(\Omega)^d$ and $L^d(\Omega)^d$. We refer the reader to [64] and [41] for a study of this formulation, and especially to [64] for the definition of an external trace and the meaning of Dirichlet boundary conditions. We only recall the following existence theorem.

THEOREM 2.2. *Let Ω be a smooth domain of class C^2. Assume $f \in L^\infty(\Omega)^d$ and $g \in L^\infty(\Gamma_N)^d$. If Γ_0 is not empty and the following safe-load condition is fulfilled:*

$$\exists \bar\sigma \in S(f,g),\ \epsilon > 0 \text{ such that } \forall \xi \in \mathbb{M}^d_s \text{ with } |\xi| \le \epsilon,\ \bar\sigma(x) + \xi \in K_M \text{ a.e. in } \Omega, \tag{14}$$

then the displacement problem (13) *has a solution in $u \in BD(\Omega)$.*

Remark 2.3. Note that there is no uniqueness of the displacement and that a counterexample can be found in [64].

3. Regularizations. As far as shape optimization is concerned, it is crucial to work on well-posed problems, which is not the case in perfect plasticity for the displacement u. This is the reason why a large part of the literature on shape optimization focuses on the formulation (8). Moreover, if we want to use a gradient-type algorithm, the solutions need to be differentiable with respect to the shape. This is clearly not the case in our problem, at least because of the projection formulation. So we have to cope with two different problems: the first is the fact that the problem does not have a unique solution, and the second comes from the fact that the problem is not differentiable with respect to the shape.

We propose two ways to address these two difficulties. These two ways involve the projection $P_K^{A^{-1}}$, which has to be regularized. As an analytic expression is known for the particular case of the von Mises criterion, we restrict ourselves to this criterion. From now on the function $\mathcal{F}$ is

$$\mathcal{F}(\sigma) = \sqrt{\sigma_D : \sigma_D} - \sigma_c = |\sigma|_D - \sigma_c, \tag{15}$$

where, for a symmetric tensor σ, its deviatoric part σ_D and hydrostatic part σ_H are defined, respectively, by

$$\sigma_D = \sigma - \frac{Tr(\sigma)}{d} I\,, \quad \sigma_H = \frac{Tr(\sigma)}{d} I\,.$$

Then the projection is

$$P_K^{A^{-1}}(\tau) = \tau - \max\left(0, 1 - \frac{\sigma_c}{|\tau_D|}\right)\tau_D. \tag{16}$$

It is now easy to regularize this projection by introducing a regularization of the function $x \to \max(0,x)$ which we note f_γ, $\gamma > 0$, being a regularization parameter. Here, we choose

$$f_\gamma(x) = \begin{cases} \frac{1}{4\gamma}x^2 + \frac{1}{2}x + \frac{\gamma}{4}, & x \in [-\gamma, \gamma]\,, \\ \max(x,0) & \text{otherwise,} \end{cases} \tag{17}$$

and the regularized projection is

$$P_K^\gamma(\tau) = \tau - f_\gamma\left(1 - \frac{\sigma_c}{|\tau_D|}\right)\tau_D. \tag{18}$$

For the sake of simplicity, the pointwise convex set K_M, defined by (5), is denoted by K in what follows when no confusion can arise.

3.1. Perzyna penalization.

3.1.1. Formulation of the problem. To introduce the Perzyna penalization, we use the Moreau–Yosida approximation [56] of the indicator function of K in (7), $\mathbb{1}_K^\eta$:

(19)
$$\mathbb{1}_K^\eta(\sigma) = \frac{1}{2\eta}\int_\Omega A^{-1}\left(\sigma - P_K^{A^{-1}}(\sigma)\right) : \left(\sigma - P_K^{A^{-1}}(\sigma)\right)\, dx = \frac{1}{2\eta}\left\|\sigma - P_K^{A^{-1}}(\sigma)\right\|^2_{A^{-1}}.$$

From (19) we can deduce an approximation for the condition $e_p \in \partial\mathbb{1}_K(\sigma)$. As $\sigma \to \mathbb{1}_K^\eta(\sigma)$ is Fréchet differentiable (see Theorem 4.1 in [75]), its subdifferential reduces to its gradient, and we can write the following pointwise formula for the approximation e_p^η:

$$e_p^\eta = \frac{1}{\eta}A^{-1}\left(\sigma - P_K^{A^{-1}}(\sigma)\right). \tag{20}$$

This directly leads to the following system of variational equations by integration of the plasticity equations (6), replacing the condition on e_p by (20):

$$\begin{cases} \displaystyle\int_\Omega \sigma^\eta : e(v)\, dx = \int_\Omega f\cdot v\, dx + \int_{\Gamma_N} g\cdot v\, ds \ \ \forall v \in H^1_{\Gamma_0}(\Omega)^d, \\ \displaystyle\int_\Omega A^{-1}\sigma^\eta : \tau\, dx + \frac{1}{\eta}\int_\Omega A^{-1}\left(\sigma^\eta - P_K^{A^{-1}}(\sigma^\eta)\right) : \tau\, dx = \int_\Omega e(u^\eta) : \tau\, dx \\ \quad \forall \tau \in L^2(\Omega;\mathbb{M}^d_s). \end{cases} \tag{21}$$

This also gives rise to further simplification of the problem (21), which is a mixed variational problem. Indeed, as we shall now show, the variable σ can be eliminated. From (20) we can deduce the expression of σ^η,

$$\sigma^\eta = Ae(u^\eta) - \frac{1}{\eta}\left(\sigma^\eta - P_K^{A^{-1}}(\sigma^\eta)\right).$$

This expression says that $Ae(u^\eta)$ is on the ray defined by σ^η and its projection $P_K^{A^{-1}}(\sigma^\eta)$. So it implies that [56, Chapter 3, Lemma 3.2]

$$P_K^{A^{-1}}(\sigma^\eta) = P_K^{A^{-1}}(Ae(u^\eta)). \tag{22}$$

This enables us to write σ^η with respect to only u^η and transform the implicit definition into an explicit one as follows:

$$\sigma^\eta = \frac{\eta}{1+\eta}Ae(u^\eta) + \frac{1}{1+\eta}P_K^{A^{-1}}(Ae(u^\eta)). \tag{23}$$

We can write the new nonlinear variational equation of the Perzyna visco–elasto-plasticity:

$$\begin{aligned} &\int_\Omega \left(\frac{\eta}{1+\eta}Ae(u^\eta) + \frac{1}{1+\eta}P_K^{A^{-1}}(Ae(u^\eta))\right) : e(v)\, dx \\ &= \int_\Omega f\cdot v\, dx + \int_{\Gamma_N} g\cdot v\, ds \ \forall v \in H^1_{\Gamma_0}(\Omega)^d. \end{aligned} \tag{24}$$

It remains to regularize the projection $P_K^{A^{-1}}$, replacing it by P_K^γ defined by (18), as follows: find $u_\eta^\gamma \in H^1_{\Gamma_0}(\Omega)^d$ such that

$$\begin{aligned}&\int_\Omega \left(\frac{\eta}{1+\eta} Ae(u_\eta^\gamma) + \frac{1}{1+\eta} P_K^\gamma(Ae(u_\eta^\gamma))\right) : e(v)\,dx \\ &= \int_\Omega f\cdot v\,dx + \int_{\Gamma_N} g\cdot v\,ds \ \forall v \in H^1_{\Gamma_0}(\Omega)^d\end{aligned} \tag{25}$$

or, in a mixed form, find $\sigma_\gamma^\eta \in L^2_s(\Omega)^{d\times d}$ and $u_\gamma^\eta \in H^1_{\Gamma_0}(\Omega)^d$ such that

$$\begin{cases} \displaystyle\int_\Omega \sigma_\gamma^\eta : e(v)\,dx = \int_\Omega f\cdot v\,dx + \int_{\Gamma_N} g\cdot v\,ds \ \ \forall v \in H^1_{\Gamma_0}(\Omega)^d \\ \displaystyle\int_\Omega A^{-1}\sigma_\gamma^\eta : \tau\,dx + \frac{1}{1+\eta}\int_\Omega A^{-1} f_\gamma\left(1 - \frac{\sigma_c}{|\sigma_\gamma^\eta|_D}\right)(\sigma_\gamma^\eta)_D : \tau\,dx \\ \displaystyle= \int_\Omega e(u_\gamma^\eta) : \tau\,dx \ \ \forall \tau \in L^2(\Omega;\mathbb{M}^d_s). \end{cases} \tag{26}$$

3.1.2. Mathematical analysis. We give two theorems stating that the solution of (25) exists, is unique, and converges to a solution of the Hencky model. For the existence and uniqueness, the proof is the same as that for Proposition 2.8 in [26] with hardening.

THEOREM 3.1. *Under the safe-load condition* (14), $f \in L^2(\Omega)^d$, *and* $g \in L^2(\Gamma_N)^d$, *there exists a unique solution* $(\sigma_\eta^\gamma, u_\eta^\gamma) \in L^2(\Omega;\mathbb{M}^d_s) \times H^1_{\Gamma_0}(\Omega)^d$ *to the problem* (25).

THEOREM 3.2. *Under the safe-load condition* (14) *and with* $f \in L^d(\Omega)^d$ *and* $g \in C^0(\Gamma_N)^d$, *when* $\eta \to 0$ *and* $\gamma \to 0$,

- σ_γ^η *converges strongly in* $L^2(\Omega;\mathbb{M}^d_s)$ *to* σ, *the stress tensor solution of the Hencky model* (13).
- *up to a subsequence,* u_γ^η *converges weakly in* $L^{\frac{d}{d-1}}(\Omega;\mathbb{R}^d)$ *and weakly in* $BD(\Omega)$ *to* u, *the displacement solution of the Hencky model* (13).

Proof. The proof is a variation of that in [41, Chapter 2] and can be found in [42]. ∎

3.2. A second regularization for the von Mises criterion.

3.2.1. Mathematical analysis. Another way to get a compatible model with shape optimization is to focus on the formulation (12), used in numerical applications, and address its nonsmoothness and ill-posedness.

DEFINITION 3.3. *Let* T *be the operator defined by*

$$T : \ u \in H^1_{\Gamma_0}(\Omega)^d \to T(u) \in \left(H^1_{\Gamma_0}(\Omega)^d\right)^*,$$

where $T(u)$ *is defined for every* $v \in H^1_{\Gamma_0}(\Omega)^d$ *as*

$$\langle T(u), v\rangle = \int_\Omega P_K^{A^{-1}}(Ae(u)) : e(v)\,dx.$$

Clearly T is monotone but is not coercive. To gain these two properties and the smoothness, we define the following regularized projection:

$$P_\gamma(\tau) = (1+\gamma)\,\tau - f_\gamma\left(1 - \frac{\sigma_c}{|\tau_D|}\right)\tau_D. \tag{27}$$

DEFINITION 3.4. *Let T_γ be the operator defined by*

$$T_\gamma \,:\, u \in H^1_{\Gamma_0}(\Omega)^d \to T_\gamma(u) \in \left(H^1_{\Gamma_0}(\Omega)^d\right)^*,$$

where $T_\gamma(u)$ is defined for every $v \in H^1_{\Gamma_0}(\Omega)^d$ as

$$\langle T_\gamma(u), v\rangle = \int_\Omega P_\gamma(Ae(u)) : e(v)\, dx.$$

The function f_γ in (27) is defined by (17). Then a regularization of (11) is simply

$$\sigma = P_\gamma\left(Ae\left(u\right)\right).$$

3.2.2. Mathematical analysis. The study of the operator T_γ is done in [42, Theorem 6.2.9 (strict monotonicity), Theorem 6.2.10 (coercivity), Lemma 6.2.11 (hemicontinuity), and Lemma 6.2.12 (boundedness)] . A simple application of Theorem 2.14 in [55] gives the following.

THEOREM 3.5. *The regularized problem is as follows: find $u_\gamma \in H^1_{\Gamma_0}(\Omega)^d$ such that*

$$\int_\Omega P_\gamma\left(Ae\left(u_\gamma\right)\right) : \epsilon(v)\, dx = \int_\Omega f\cdot v\, dx + \int_{\Gamma_N} g\cdot v\, ds \;\forall v \in H^1_{\Gamma_0}(\Omega)^d \tag{28}$$

admits a unique solution. The associated regularized stress tensor is defined as

$$\sigma_\gamma = P_\gamma\left(Ae\left(u_\gamma\right)\right).$$

Then it is proved in [42, Theorems 6.2.15 and 6.2.16] that the solution of the regularized problem (28) converges to the solution of the Hencky problem, as the regularization parameter goes to zero.

THEOREM 3.6. *Under the safe-load condition* (14) *and with $f \in L^d(\Omega)^d$ and $g \in C^0(\Gamma_N)^d$,*

- *the solution σ_γ converges, as γ goes to 0, strongly in $L^2(\Omega;\mathbb{M}^d_s)$ to σ, the stress tensor solution of the Hencky model.*
- *the solution u_γ converges weakly, up to a subsequence, in $L^{\frac{d}{d-1}}(\Omega;\mathbb{R}^d)$ and weakly in $BD(\Omega)$ to a displacement u solution to the Hencky model.*

3.3. Conclusion on the two proposed regularizations. For the von Mises criterion, the two formulations introduced in this section are quite similar. They are tantamount to redefining σ by one of the following formulae:

1. For the Perzyna penalization,

$$\sigma = Ae(u) - \frac{1}{1+\eta} f_\gamma\left(1 - \frac{\sigma_c}{|Ae(u)|_D}\right)\left(Ae(u)\right)_D.$$

2. For the second regularization,

$$\sigma = (1+\gamma)Ae(u) - f_\gamma\left(1 - \frac{\sigma_c}{|Ae(u)|_D}\right)\left(Ae(u)\right)_D.$$

In each case, the problem reduces to a nonlinear variational equation as follows: find $u \in H^1_{\Gamma_0}(\Omega)^d$ such that

$$\int_\Omega \sigma : e(v)\, dx = \int_\Omega f\cdot v\, dx + \int_{\Gamma_N} g\cdot v\, ds \quad \forall v \in H^1_{\Gamma_0}(\Omega)^d. \tag{29}$$

4. Derivation and optimization. Our goal is to minimize an objective function $J(\Omega)$ depending on u, the displacement which solves one of the formulations given in section 3 under constraints noted $C(\Omega)$ also depending on u:

$$\begin{cases} \min J(\Omega), \\ \Omega \in \mathcal{U}_{ad}, \\ u \text{ solution of (29)}, \\ C(\Omega) \leq 0, \end{cases} \tag{30}$$

where $\mathcal{U}_{ad}$ is the set of admissible shapes. These shapes should be included in a fixed domain D, $\Omega \subset D$, as follows, and the Dirichlet boundary $\Gamma_0 \subset \partial D$ is not allowed to change:

$$\mathcal{U}_{ad} = \{\Omega \subset D \text{ bounded and open such that } \Gamma_0 \subset \partial D \text{ is fixed}\}.$$

In the following we denote by Γ_m the part of the boundary of Ω which is allowed to change. Examples of typical functions $J(\Omega)$ and $C(\Omega)$ are given in Remark 4.6.

4.1. Shape derivative. To minimize (30) we apply a gradient method, which relies on the notion of a Hadamard shape derivative for functionals depending on the domain Ω; see, for instance, [23], [47], [51], [61], or [62]. Starting from a smooth domain Ω_0, the variation of the domain takes the form

$$\Omega_\theta = (Id + \theta)(\Omega_0),$$

with $\theta \in W^{1,\infty}(\mathbb{R}^d, \mathbb{R}^d)$ and Id the identity map. When θ is sufficiently small, $Id + \theta$ is a diffeomorphism in $\mathbb{R}^d$; see [2]. Once the variation of the shape is defined, it is possible to define the notion of a Gâteaux derivative for a function J depending on the shape.

DEFINITION 4.1. *The shape derivative $J'(\Omega)(\theta)$ of $J(\Omega)$ at Ω in the direction θ is defined as the derivative at 0 of the application $t \to J((Id + t\theta)(\Omega))$, which means that*

$$J((Id + t\theta)(\Omega)) = J(\Omega) + tJ'(\Omega)(\theta) + o(t),$$

where $J'(\Omega)$ is a continuous linear form on $W^{1,\infty}(\mathbb{R}^d, \mathbb{R}^d)$.

We recall the following classical theorem [2], which will be used in the next section.

THEOREM 4.2. *Let Ω be a smooth open set, ϕ a smooth function defined in $\mathbb{R}^d$,*

$$J_v(\Omega) = \int_\Omega \phi(x)\, dx \quad \text{and} \quad J_s(\Omega) = \int_{\partial\Omega} \phi(x)\, ds.$$

These two functions are shape differentiable at Ω in the direction $\theta \in W^{1,\infty}(\mathbb{R}^d, \mathbb{R}^d)$ and

$$J_v'(\Omega)(\theta) = \int_{\partial\Omega} \theta \cdot n\phi\, ds \quad \text{and} \quad J_s'(\Omega)(\theta) = \int_{\partial\Omega} \theta \cdot n \left(\frac{\partial\phi}{\partial n} + H\phi\right) ds,$$

where $H = \operatorname{div}(n)$ is the mean curvature of $\partial\Omega$.

4.2. Differentiability of the regularized formulation. As far as optimization is concerned, we need to investigate the differentiability of the operator $\tau \to f_\gamma(1 - \frac{\sigma_c}{|\tau|_D})$. As f_γ is a smooth Lipschitz function from $\mathbb{R}$ to $\mathbb{R}$, it is Gâteaux differentiable pointwise. It has no chance to be Fréchet differentiable from $L^2(\Omega)$ to $L^2(\Omega)$.

LEMMA 4.3. *There exists $\delta > 0$ such that the solution u of the problem* (29) *belongs to $W^{1,p}(\Omega)^d$, with $p \in [2, \overline{p}]$ and $\overline{p} = 2 + \delta > 2$. Moreover $\tau \to f_\gamma(1 - \frac{\sigma_c}{|\tau|_D})$ is Fréchet differentiable from $L^{2+\delta}(\Omega)$ to $L^2(\Omega)$.*

Proof. The regularity of u is given by Theorem 1.1 of [25]. The Fréchet differentiability of f_γ is shown in [26]. ∎

This lemma implies that both regularizations are Fréchet differentiable with respect to u from $W^{1,\overline{p}}(\Omega)^d$ to $H^1(\Omega)^d$.

4.3. Computation of the gradients. We proceed now to the computation of the gradient of a general criterion:

$$J(\Omega) = \int_\Omega m(u)\,dx + \int_{\partial\Omega} l(u)\,ds, \tag{31}$$

where u is solution of (29), Γ_m is the part of $\partial\Omega$ which is allowed to move during the optimization process, and m and l are smooth functions from $\mathbb{R}^d$ to $\mathbb{R}$, satisfying the growth conditions

$$|m(u)| \le C\left(1 + |u|^2\right), \quad |m'(u)\cdot h| \le C\,|u|\;|h|$$

and

$$|l(u)| \le C\left(1 + |u|^2\right), \quad |l'(u)\cdot h| \le C\,|u|\;|h|$$

for every $h \in L^2(\Omega)^d$ and $u \in L^2(\Omega)^d$.

THEOREM 4.4. *Assume that $\Gamma_m \cap \Gamma_0 = \emptyset$, that $f \in H^1(\mathbb{R}^d)^d$ and $g \in H^2(\mathbb{R}^d)^d$, and that u is solution of* (29). *The function $J(\Omega)$, defined by* (31), *is shape differentiable, and its shape derivative is given by*

$$\begin{aligned} J'(\Omega)(\theta) = &\int_{\Gamma_m} \theta\cdot n\Big(m(u) - f\cdot p\Big)\,ds \\ &+ \int_{\Gamma_m} \theta\cdot n\Big(Hl(u) + \partial_n l(u)\Big) \\ &- \int_{\Gamma_N\cap\Gamma_m} \theta\cdot n\Big(Hp\cdot g + \partial_n(p\cdot g)\Big)\,ds \\ &+ \int_{\Gamma_m} \theta\cdot n\Big(\sigma : e(p)\Big), \end{aligned} \tag{32}$$

where $p \in H^1_{\Gamma_0}(\Omega)^d$ is defined as the solution of the following adjoint problem:

$$\begin{aligned} &\alpha\int_\Omega Ae(p) : e(\psi)\,dx - \beta\int_\Omega f_\gamma\left(1 - \frac{\sigma_c}{|Ae(u)|_D}\right)(Ae(p))_D : e(\psi)_D\,dx \\ &-\beta\int_\Omega f'_\gamma\left(1 - \frac{\sigma_c}{|Ae(u)|_D}\right)\frac{\sigma_c}{|Ae(u)|^3_D}Ae(u)_D : Ae(\psi)_D\;Ae(u)_D : e(p)_D\,dx \\ &= -\int_\Omega m'(u)\cdot\psi\,dx - \int_{\partial\Omega} l'(u)\cdot\psi\,ds \quad \forall\psi \in H^1_{\Gamma_0}(\Omega)^d, \end{aligned} \tag{33}$$

with

- $\alpha = 1$ *and* $\beta = 1/(1+\eta)$ *for the Perzyna regularization,*
- $\alpha = 1+\eta$ *and* $\beta = 1$ *for the second regularization.*

Remark 4.5. The adjoint problem (33) is well-posed for both regularizations using the function (17). This is ensured by the coercivity of the associated bilinear form. To prove it, it suffices to analyze the three possible cases which can occur: $1 - \frac{\sigma_c}{|Ae(u)|_D} \in [-\infty, -\gamma]$, $1 - \frac{\sigma_c}{|Ae(u)|_D} \in [-\gamma, \gamma]$, and $1 - \frac{\sigma_c}{|Ae(u)|_D} \in [\gamma, +\infty[$.

Proof. The proof is classical and relies on Céa's Lagrangian method; see [7] or [2]. To make it fully rigorous would require first to prove that the solution u of (29) is Gâteaux differentiable with respect to the shape. This is a well-known result; we briefly recall the main arguments. First, the variational formulation (29) is rewritten in the reference configuration Ω_0 using a change of variables such that $\Omega = (Id + t\theta)(\Omega_0)$. This leads to a functional equation of the type $F(u,t) = 0$, with F differentiable with respect to t. Second, applying the implicit function theorem at $t = 0$ yields the desired result (see [23] if necessary). Denoting by $u'(\theta)$ the shape derivative of u, we now prove the theorem by the Lagrangian method. Let us introduce the Lagrangian L, defined for any v and q in $H^1_{\Gamma_0}(\mathbb{R}^d)^d$ (the space of functions defined in $\mathbb{R}^d$ which vanishes on Γ_0; recall that Γ_0 is not allowed to move):

$$
\begin{aligned}
L(v,q,\Omega) \quad = \quad & \int_\Omega m(v)\,dx + \int_\Gamma l(v)\,ds + \alpha \int_\Omega Ae(v) : e(q)\,dx \\
& -\beta \int_\Omega f_\gamma \left(1 - \frac{\sigma_c}{|Ae(v)|_D}\right) (Ae(v))_D : e(q)_D\,dx \\
& - \int_\Omega f \cdot q\,dx - \int_{\Gamma_N} g \cdot q\,ds,
\end{aligned} \tag{34}
$$

with α and β depending on the model chosen as stated in Theorem 4.4. Since Γ_0 is fixed, we do not need a Lagrange multiplier for the Dirichlet condition in the Lagrangian: $\Gamma_0 \subset \partial\Omega$ for every $\Omega \in \mathcal{U}_{ad}$. Moreover the functions q and v are in spaces independent of $\Omega \in \mathcal{U}_{ad}$. Let (u,p) be a stationarity point of L. The state equation (29) can be retrieved by differentiating L with respect to q in the direction $\psi \in H^1_{\Gamma_0}(\mathbb{R}^d)^d$:

$$\langle \partial_q L(u,q,\Omega), \psi \rangle = 0 \quad \forall \psi \in H^1_{\Gamma_0}(\mathbb{R}^d)^d.$$

In the same way, the adjoint equation solved by p can be found by derivating L with respect to v in the direction $\psi \in H^1_{\Gamma_0}(\mathbb{R}^d)^d$:

$$
\begin{aligned}
\langle \partial_u L, \psi \rangle = {} & \alpha \int_\Omega Ae(p) : e(\psi)\,dx - \beta \int_\Omega f_\gamma \left(1 - \frac{\sigma_c}{|Ae(u)|_D}\right) (Ae(p))_D : Ae(\psi)_D\,dx \\
& + \int_\Omega m'(u) \cdot \psi\,dx + \int_{\Gamma_m} l'(u) \cdot \psi\,ds \\
& - \beta \int_\Omega f'_\gamma \left(1 - \frac{\sigma_c}{|Ae(u)|_D}\right) \frac{\sigma_c}{|Ae(u)|^3_D} Ae(u)_D : Ae(\psi)_D\ Ae(u)_D : e(p)_D\,dx,
\end{aligned}
$$

and the adjoint problem can be deduced:

$$\langle \partial_u L(u,p,\Omega), \psi \rangle = 0 \quad \forall \psi \in H^1_{\Gamma_0}(\mathbb{R}^d),$$

which gives (33). In regard to finding the shape derivative of $J(\Omega)$, we remark that, for any $q \in H^1_{\Gamma_0}(\mathbb{R}^d)^d$,

$$J(\Omega) = L(u(\Omega), q, \Omega),$$

and differentiate it with respect to the shape in the direction θ, which gives

$$J'(\Omega)(\theta) = L'(\Omega, u_\Omega, q)(\theta) = \partial_\Omega L(\Omega, u_\Omega, q)(\theta) + \langle \partial_u L(\Omega, u_\Omega, q), u'(\theta)\rangle.$$

But as $u'(\theta)$ belongs to $H^1_{\Gamma_0}(\Omega)^d$, taking $q = p(\Omega)$ leads to

$$\langle \partial_u L(\Omega, u_\Omega, p(\Omega)), u'(\theta)\rangle = 0.$$

Consequently,

$$J'(\Omega, \theta) = \partial_\Omega L(\Omega, u_\Omega, p_\Omega)(\theta),$$

and using the formulae of Theorem 4.2, we deduce the desired result (32). ∎

Remark 4.6. Our optimization problem (30) involves an objective function $J(\Omega)$ and a constraint $C(\Omega)$. Both functions are of the type (31), and we now specify the previous formulas for the integrands m and l. The objective function $J(\Omega)$ is the volume, corresponding to

$$m_{vol}(u) = 1,$$

$$l_{vol}(u) = 0.$$

The constraint $C(\Omega)$ is a criterion on the displacement, restricted to that part of the boundary where the force is applied, namely,

$$m_{Disp}(u) = 0,$$

$$l_{Disp}(u) = |u|^2 \mathbb{1}_{\Gamma_N}.$$

5. Numerical implementation.

5.1. The level set method. For numerical purposes our shapes are defined by level set functions, following the framework introduced by Osher and Sethian [49]; see also [48] and [59]. Let $D \subset \mathbb{R}^d$ be a bounded domain in which all admissible shapes Ω are included. The boundary of Ω is located by virtue of the level set function ψ, defined in D by

$$\begin{cases} \psi(x) = 0 & \text{if } x \in \partial\Omega \cap D, \\ \psi(x) < 0 & \text{if } x \in \Omega, \\ \psi(x) > 0 & \text{otherwise.} \end{cases}$$

The normal n and the mean curvature H of the shape Ω are respectively given by $\frac{\nabla\psi}{|\nabla\psi|}$ and $\mathrm{div}(\frac{\nabla\psi}{|\nabla\psi|})$. These quantities are computed throughout the whole domain D, which naturally defines extensions of their definition on $\partial\Omega$.

5.2. Optimization algorithm. This algorithm is similar to that introduced in [3] for a model of linearized elasticity, and the reader is referred to [3] for details on numerical implementation. The optimization process produces iteratively a sequence $(\Omega_i)_{i\in\mathbb{N}}$ of shapes, starting from an initial shape Ω_0. The level set function is evolved from Ω_i to Ω_{i+1} by solving the following Hamilton–Jacobi transport equation [49] for $t \in [0, t_f]$:

$$\frac{\partial\psi}{\partial t} + V|\nabla\psi| = 0 \text{ in } D, \tag{35}$$

where $\psi(0,x)$ is a level set function for Ω_i and $V(x)$ is the normal velocity of the shape's boundary. This normal velocity V can be identified with $\theta \cdot n$, where θ is a direction of derivation which makes the shape derivative of section 4 negative. Note that since shape derivatives are defined as integrals on the boundary $\partial\Omega$, the normal velocity V must be extended to the whole computational domain D. In the meantime, it is also regularized (see, e.g., the end of section 3 in [3]). For a constrained optimization problem like (30), we could apply this procedure as such for the Lagrangian, deduce V from the shape derivative of the Lagrangian, and update the Lagrange parameters at each optimization iteration. However, for efficiency reasons, we prefer to rely on a sequential linear programming (SLP) type algorithm. More precisely, computing shape derivatives of the objective function and of the constraints (using Theorem 4.4), we linearize (30) and, adding a trust region constraint, solve this linear program using the `qld` routine in Scilab [58] (a linear quadratic programming solver) to deduce a descent direction which, after extension to D, is precisely the normal velocity V.

The final time t_f for (35) can be interpreted as a descent step. It is initialized as a given value $t_{\max}$ and then decreases until an admissible shape is found (if not, the algorithm stops). When an admissible shape is accepted, the time step t_f is allowed to grow. We distinguish two phases in the algorithm. First, if the current shape does not fulfill the constraints, we allow the objective to slowly increase as long as the constraints improve. Then, once an admissible shape is reached, we reject every future shape, which either makes the objective increase or is not admissible. The new shape Ω_{i+1} is defined by the final level set function $\psi(t_f,x)$.

The Hamilton–Jacobi equation (35) is solved by an explicit second-order upwind scheme on a Cartesian grid of D with Neumann boundary conditions. Since the scheme is explicit in time, the time stepping has to satisfy a CFL condition and, in order to regularize the level set which can become too flat or too steep during the successive optimization iterations, periodic reinitializations are performed.

5.3. Finite element method. On the same Cartesian grid we solve the mechanical system (29) and the adjoint system (33) using bilinear quadrangular (Q1) finite elements. Such a choice is made, for example, in [73] and [60] and in [53], where perfect plasticity is solved in the static case and some a posteriori estimates are given. For the two regularized models proposed in this paper, a numerical study is made on their convergence to the Hencky model in [42] (see Chapter 4, section 4.5.2 for the Perzyna model and Chapter 6, section 6.2.2 for the other model, using a particular example). Tables with L^2 errors on σ and u are given in [42] as well as tables showing the realization of the constraint $\sigma \in K$. As is well known, using quadrangular elements in the framework of shape optimization can have some drawbacks [65] such as the appearance of checkerboard patterns and one-node connections. However, because of the chosen optimization problems, we never find one-node connections in the present study, and there are no checkerboards with the level set method.

To avoid meshing the shapes Ω, we rely on the "ersatz material" approach which fills $D \setminus \Omega$ with a weak material mimicking void but preventing the stiffness matrix from being singular. This technique is commonly used in topology optimization with level sets [3], [70].

Concerning the nonlinear penalized equations, they are usually solved by a damped Newton method (see [12, Chapter 6]) or a fixed point method. The Newton method has the advantage of being faster but it needs a good choice for the damping. On the other hand, the fixed point method, despite its relative slowness, is easier to imple-

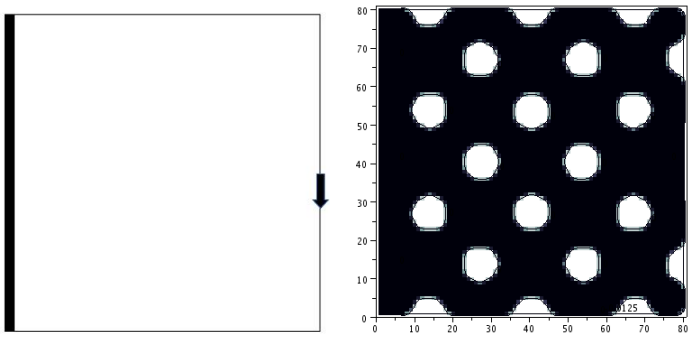

(a) Load case. (b) Initialization.

FIG. 3. *Cantilever: problem definition.*

TABLE 1
Results for the cantilever.

Case	Volume	Displacement	Constraint	Iter.	Eval.
Elastic	1.35746	7.99968e-07	8e-07	32	56
Perzyna	2.42645	7.99909e-07	8e-07	28	51
Sec. Reg.	2.42656	7.99909e-07	8e-07	28	51

ment. The robustness of the algorithm which solves the direct problem is crucial in the optimization process because the optimization can produce structures for which the finite element matrices are nearly singular. Here we choose to use a fixed point method for the computation of the nonlinear problems, which converges in, at most, 300 iterations with an average of 100.

6. Numerical examples. We consider five two-dimensional examples. In all examples the regularization parameters are $\eta = \gamma = 10^{-10}$. There are no volume forces but only surface loadings. In every example a small amount of material is forced to remain near the loading and clamped boundaries (these zones cannot be optimized). As a consequence, all shapes exhibit a material layer along the Dirichlet and non-homogeneous Neumann boundaries. For all examples the volume is minimized under an inequality constraint on the displacement (see Remark 4.6 for a precise definition). For each example, the value of the constraint can be found in the column "Constraint" of the corresponding table.

6.1. Cantilever. For this example we use a grid mesh of 6400 Q1-elements. The design domain D has a length and a height of 2. A constant vertical force equal to 1.1 is applied on the middle right (from $(2, 0.9)$ to $(2, 1.1)$), and the left side is clamped (see Figure 3). The volume is optimized under a displacement constraint. The material parameters are $E = 1960$, $\nu = 0.3$, and $\sigma_c = 0.95$. Results are given in Table 1 and Figures 4 and 5.

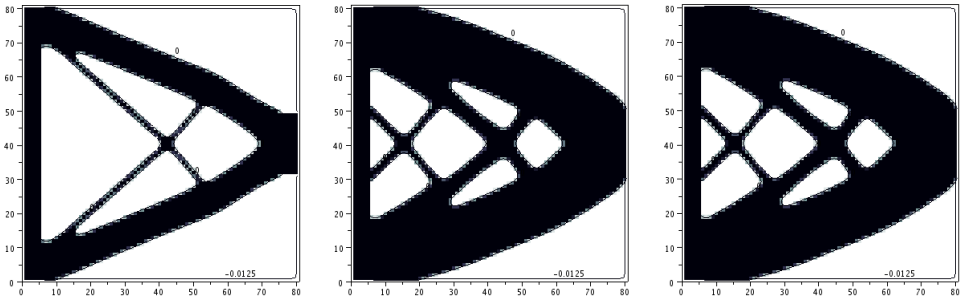

(a) Without plasticity. (b) Perzyna penalization. (c) Second regularization.

FIG. 4. *Cantilever: final designs.*

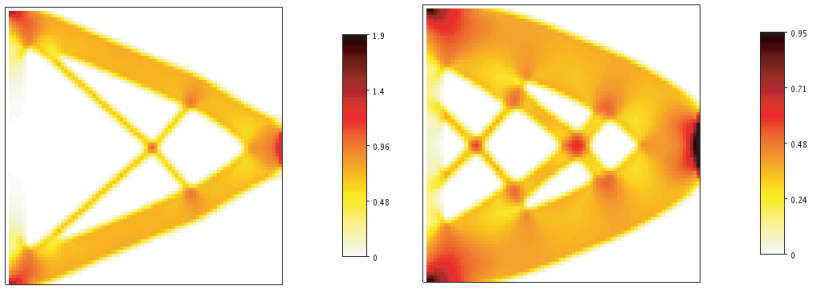

(a) von Mises effective stress for the elasticity case.

(b) von Mises effective stress for Perzyna penalization.

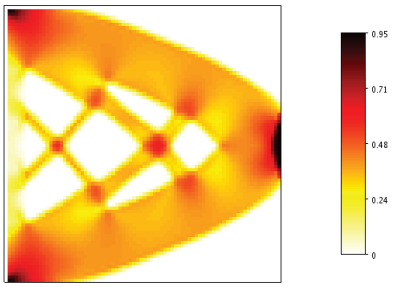

(c) von Mises effective stress for the second regularization.

FIG. 5. *Cantilever: von Mises effective stress plot for the final designs (the color scale differs between elasticity and plasticity).*

As can be expected, taking plasticity into account produces heavier structures. Indeed the algorithm tries to avoid the appearance of plastic zones, which are less rigid and induce larger displacements. Note that the two different plasticity models give a similar final design and that plasticity zones appear near the boundary conditions.

6.2. Bridge. The design domain has a length equal to 4 and a height of 1. We use a grid of 160×40 (6400) Q1-elements. The right and left sides are clamped. A constant vertical force equal to 30 is applied on the middle of the upper side from

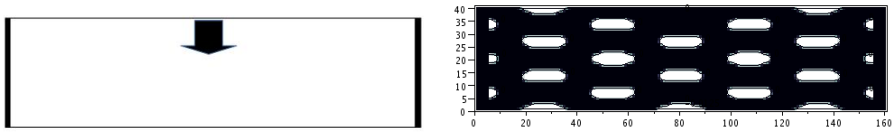

(a) Load case. (b) Initialization.

FIG. 6. *Bridge: problem definition.*

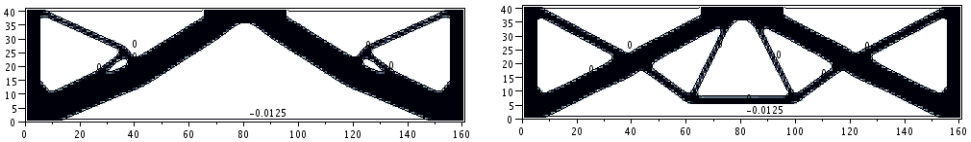

(a) Without plasticity. (b) Perzyna penalization.

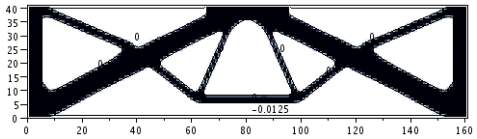

(c) Second regularization.

FIG. 7. *Bridge: final designs.*

TABLE 2
Results for the bridge.

Case	Volume	Displacement	Constraint	Iter.	Eval.
Elastic	1.39414	8.99939e-07	9e-07	47	74
Perzyna	1.38493	8.99537e-07	9e-07	42	70
Sec. Reg.	1.364	8.99995e-07	9e-07	51	81

$(1.748, 1)$ to $(2.25, 1)$ (see Figure 6). The volume is optimized under a displacement constraint. The material parameters are $E = 1.8 \times 10^5$, $\nu = 0$, and $\sigma_c = 70$, as in [57]. Results are gathered in Table 2 and Figures 7 and 8.

In this example, we note that the algorithm did not take the same path when plasticity is considered. We also remark that plasticity zones appear not only near the loading zone but also at the meeting point of different bars. The fact that, in plastic cases, the volume is lower than in the elastic case could be explained by the different paths taken by the algorithm.

6.3. Pylon 1. For this example we use a grid mesh of 6400 Q1-elements. The design domain has a length and a height of 2. The structure is fixed on the bottom right and the bottom left. A constant vertical force equal to 2 is applied on the left of the upper side from $(0.1, 2)$ to $(0.35, 2)$ (see Figure 9). The volume is optimized under a displacement constraint. The material parameters are $E = 1960$, $\nu = 0.3$, and $\sigma_c = 2$. Results are shown in Table 3 and Figures 10 and 11.

In this example, there is a clear difference between the elastic case and the plastic cases. In the elastic case, the connection with the Dirichlet conditions on the bottom right is not needed, whereas in the plastic case, it is required by the algorithm. We note also that the final values of the volume are quite the same in every case.

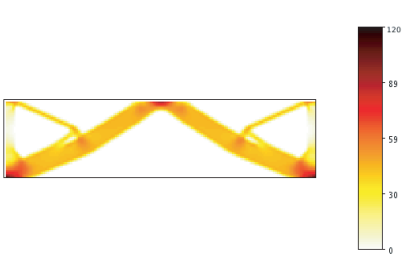

(a) von Mises effective stress for the elasticity case.

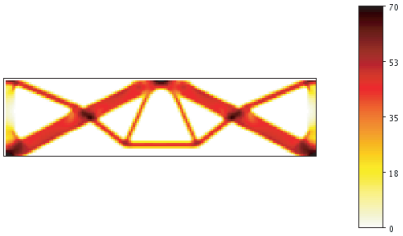

(b) von Mises effective stress for Perzyna penalization.

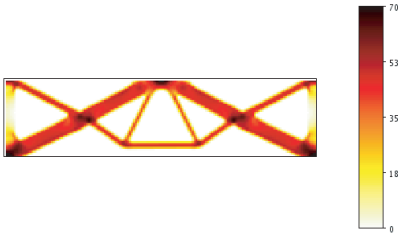

(c) von Mises effective stress for the second regularization.

FIG. 8. *Bridge: von Mises effective stress plot for the final designs (the color scale differs between elasticity and plasticity).*

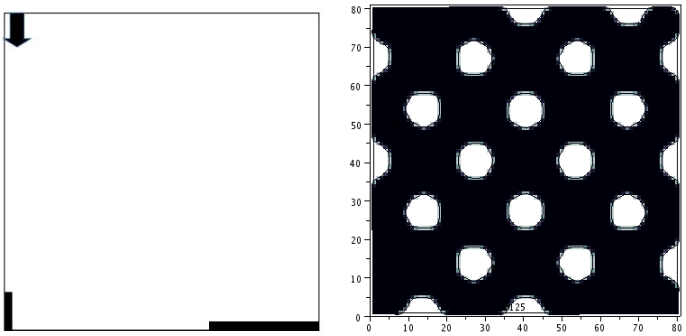

(a) Load case. (b) Initialization.

FIG. 9. *Pylon* 1: *problem definition.*

6.4. The Y. The design domain has a length equal to 2 and a height of 1. We use a grid of 160×80 (12800) Q1-elements. The left side is fixed. A constant force equal to 1.3 is applied on the top right from $(2, 0.025)$ to $(2, 0.25)$ and on the bottom right from $(2, 0.75)$ to $(2, 0.975)$ (see Figure 12). The volume is optimized under a displacement constraint. The material parameters are $E = 1960$, $\nu = 0.3$, and $\sigma_c = 1$. Results are collated in Table 4 and Figures 13 and 14.

TABLE 3
Results for the Pylon 1.

Case	Volume	Displacement	Constraint	Iter.	Eval.
Elastic	0.682463	7.99926e-07	8e-07	602	683
Perzyna	0.682525	7.9992e-07	8e-07	501	547
Sec. Reg.	0.676969	7.99838e-07	8e-07	297	349

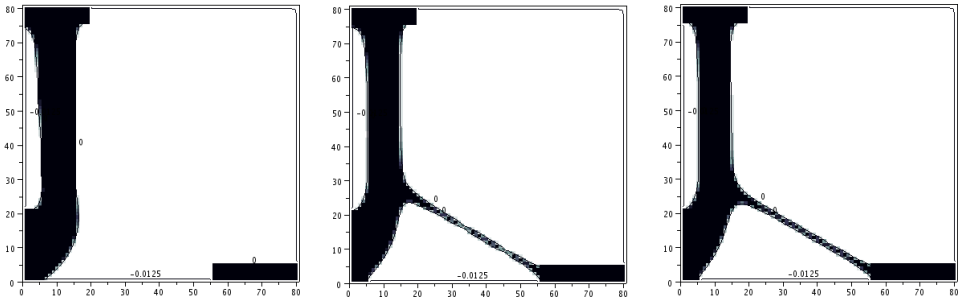

(a) Without plasticity. (b) Perzyna penalization. (c) Second regularization.

FIG. 10. *Pylon 1: final designs.*

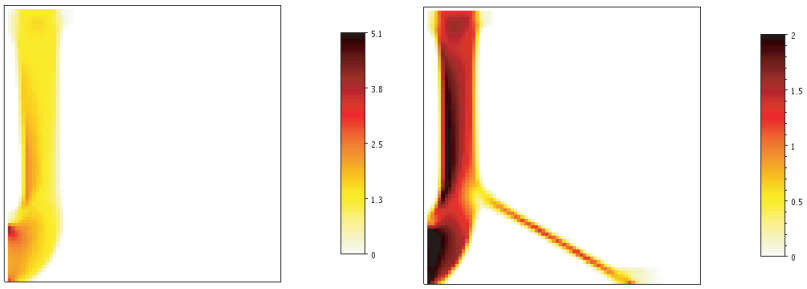

(a) von Mises effective stress for the elasticity case.

(b) von Mises effective stress for Perzyna penalization.

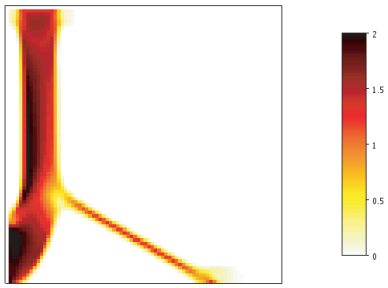

(c) von Mises effective stress for the second regularization.

FIG. 11. *Pylon 1: von Mises effective stress plot for the final designs (the color scale differs between elasticity and plasticity).*

TABLE 4
Results for the Y.

Case	Volume	Displacement	Constraint	Iter.	Eval.
Elastic	1.19588	2.99967e-07	3e-07	77	101
Perzyna	1.21094	2.99938e-07	3e-07	129	154
Sec. Reg.	1.20746	2.9913e-07	3e-07	139	163

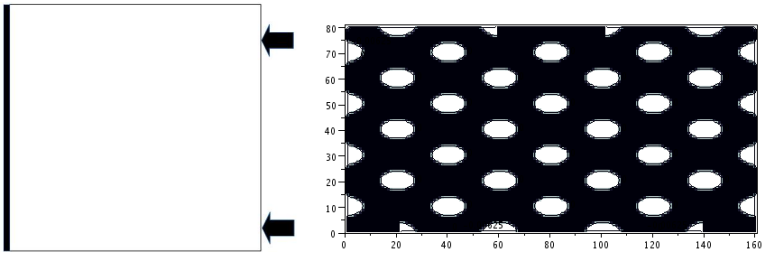

(a) Load case. (b) Initialization.

FIG. 12. *The Y.*

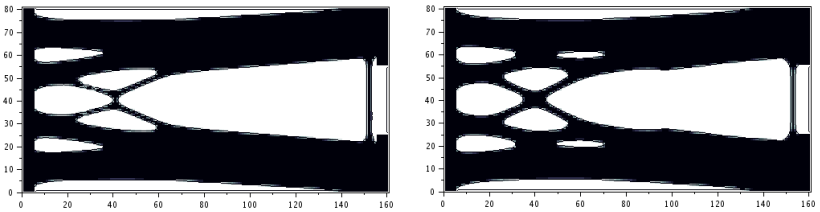

(a) Without plasticity. (b) Perzyna penalization.

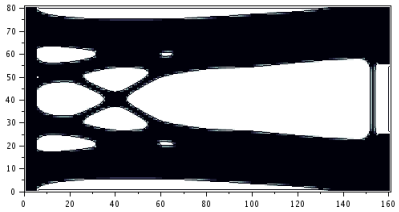

(c) Second regularization.

FIG. 13. *The Y, final designs.*

The elastic case is slightly lighter than the plastic cases. We can also remark that the crossed bars in the left middle of the structure are thinner in the elastic case, as they would probably collapse if plasticity is taken into account.

6.5. Pylon 2. The structure is fixed on the bottom left, right, and middle. The design domain has a length equal to 2 and a height of 1 (see Figure 15). We use a grid of 160×80 (12800) Q1-elements. A constant force equal to 40 is applied on the top middle from $(0.8, 1)$ to $(1.2, 1)$. The volume is optimized under a displacement constraint. For the material characteristic we take $E = 3000$, $\nu = 0$, and $\sigma_c = 70$. Results are presented in Table 5 and Figures 16 and 17.

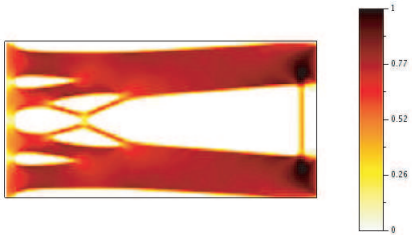

(a) von Mises effective stress for the elasticity case.

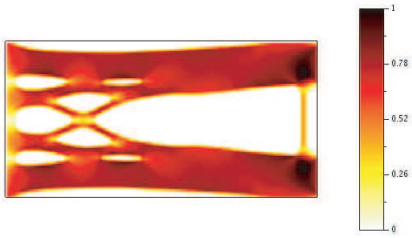

(b) von Mises effective stress for Perzyna penalization.

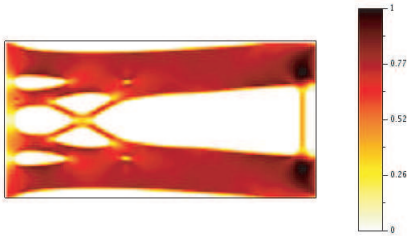

(c) von Mises effective stress for the second regularization.

FIG. 14. *The Y, von Mises effective stress for the final designs (the color scale differs between elasticity and plasticity).*

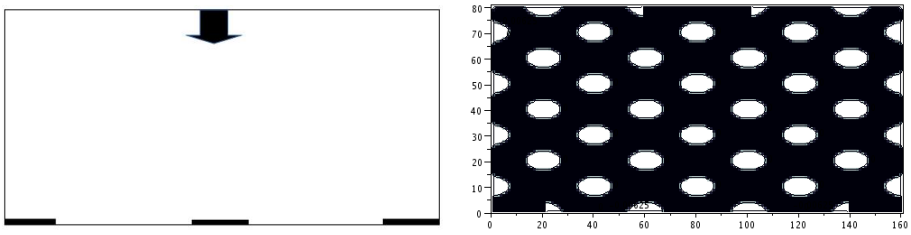

(a) Load case.

(b) Initialization.

FIG. 15. *Pylon* 2.

The volume in the elastic case is smaller than in the plastic cases. We point out that the links between the force zone and the two embedded areas on the left and right sides are practically unnecessary in the elastic case contrary to the plastic cases. Indeed, to hold, the elastic structure mostly needs the Dirichlet zone which is just facing the force no matter how small it is with respect to the dimension of the zone where the force is applied. In the plastic case, as this Dirichlet zone is four times smaller than the force zone, it leads to the appearance of a plastic area. Consequently, the plastic cases hold equally on each of the three embedded parts.

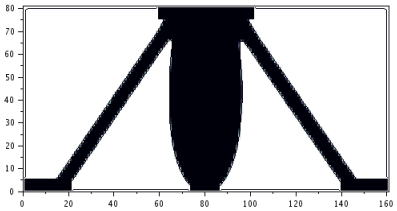

(a) Without plasticity.

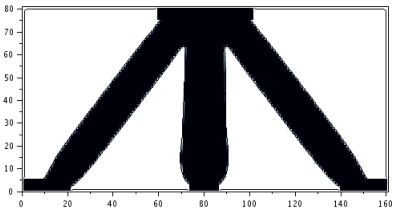

(b) Perzyna penalization.

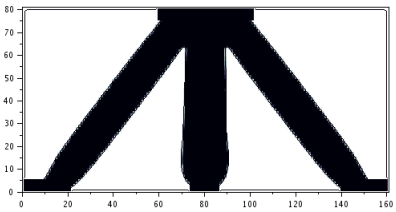

(c) Second regularization.

FIG. 16. *Pylon* 2, *final designs.*

(a) von Mises effective stress for the elasticity case.

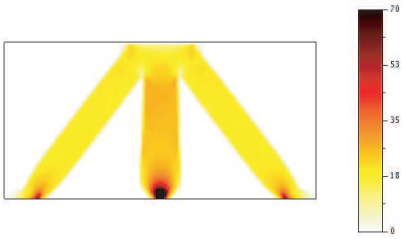

(b) von Mises effective stress for Perzyna penalization.

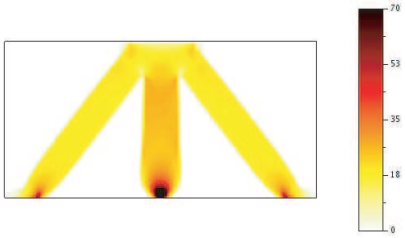

(c) von Mises effective stress for the second regularization.

FIG. 17. *Pylon* 2, *von Mises effective stress for the final designs (the color scale differs between elasticity and plasticity).*

TABLE 5
Results for the Pylon 2.

Case	Volume	Displacement	Constraint	Iter.	Eval.
Elastic	0.559843	4.99999e-07	5e-07	39	64
Perzyna	0.690667	4.99997e-07	5e-07	101	139
Sec. Reg.	0.690791	4.99999e-07	5e-07	103	143

REFERENCES

[1] B. A. Akbora, R. B. Corotis, and J. H. Ellis, *Optimization of structural frames with elastic and plastic constraints*, Civil Engrg. Syst., 10 (1993), pp. 147–169.

[2] G. Allaire, *Conception optimale de structures*, Math. Appl. (Berlin) 58, Springer-Verlag, Berlin, 2007.

[3] G. Allaire, F. Jouve, and A.-M. Toader, *Structural optimization using sensitivity analysis and a level-set method*, J. Comput. Phys., 194 (2004), pp. 363–393, https://doi.org/10.1016/j.jcp.2003.09.032.

[4] A. Bensoussan and J. Frehse, *Regularity Results for Nonlinear Elliptic Systems and Applications*, Appl. Math. Sci. 151, Springer-Verlag, 2002.

[5] T. Betz and C. Meyer, *Second-order sufficient optimality conditions for optimal control of static elastoplasticity with hardening*, ESAIM Control Optim. Calc. Var., 21 (2015), pp. 271–300.

[6] F. Brezzi and M. Fortin, *Mixed and Hybrid Finite Element Methods*, Springer Ser. Comput. Math. 15, Springer-Verlag, 1991.

[7] J. Céa, *Conception optimale ou identification de formes, calcul rapide de la dérivée directionnelle de la fonction coût*, Modél. Math. Anal. Numér., 20 (1986), pp. 371–402.

[8] G. Dal Maso, A. DeSimone, and M. G. Mora, *Quasistatic evolution problems for linearly elastic–perfectly plastic materials*, Arch. Ration. Mech Anal., 180 (2006), pp. 237–291.

[9] G. Dal Maso and R. Scala, *Quasistatic evolution in perfect plasticity as limit of dynamic processes*, J. Dynam. Differential Equations, 26 (2014), pp. 915–954.

[10] J. C. De los Reyes, *Optimization of mixed variational inequalities arising in flow of viscoplastic materials*, Comput. Optim. Appl., 52 (2012), pp. 757–784.

[11] J. C. de los Reyes, R. Herzog, and C. Meyer, *Optimal control of static elastoplasticity in primal formulation*, SIAM J. Control Optim., 54 (2016), pp. 3016–3039, https://doi.org/10.1137/130920861.

[12] J. E. Dennis, Jr., and R. B. Schnabel, *Numerical Methods for Unconstrained Optimization and Nonlinear Equations*, Classics Appl. Math. 16, SIAM, 1996, https://doi.org/10.1137/1.9781611971200. An unabridged, corrected republication of the work first published by Prentice–Hall, 1983.

[13] Z. Dimitrovová, *A new methodology to establish upper bounds on open-cell foam homogenized moduli*, Struct. Multidiscip. Optim., 29 (2005), pp. 257–271.

[14] G. Duvaut and J.-L. Lions, *Les inéquations en mécanique et en physique*, Travaux et Recherches Mathématiques 21, Dunod, Paris, 1972.

[15] W. Egner, Z. Kordas, and M. Życzkowski, *Optimal plastic shape design via the boundary perturbation method*, Struct. Optim., 8 (1994), pp. 145–155.

[16] M. Fuchs and G. Seregin, *Variational Methods for Problems from Plasticity Theory and for Generalized Newtonian Fluids*, Springer Science+Business Media, 2000.

[17] A. Grigusevicius and S. Kalanta, *Optimization of elastic-plastic beam structures with hardening using finite element method*, Found. Civil Environ. Engrg., (2005), no. 6, pp. 31–52.

[18] P. Grisvard, *Elliptic Problems in Nonsmooth Domains*, Monogr. Stud. Math. 24, Pitman, 1985.

[19] W. Han and B. D. Reddy, *Plasticity: Mathematical Theory and Numerical Analysis*, Interdiscip. Appl. Math. 9, Springer-Verlag, 2013.

[20] J. Haslinger and R. Mäkinen, *Shape optimization of elasto-plastic bodies under plane strains: Sensitivity analysis and numerical implementation*, Struct. Optim., 4 (1992), pp. 133–141.

[21] J. Haslinger and P. Neittaanmäki, *On the existence of optimal shapes in contact problems—perfectly plastic bodies*, Comput. Mech, 1 (1986), pp. 293–299.

[22] J. Haslinger, P. Neittaanmäki, and T. Tiihonen, *Shape optimization in contact problems. 1. Design of an elastic body. 2. Design of an elastic perfectly plastic body*, in Analysis and Optimization of Systems, Springer, 1986, pp. 29–39.

[23] A. Henrot and M. Pierre, *Variation et optimisation de formes. Une analyse géométrique*, Math. Appl. (Berlin) 48, Springer-Verlag, 2005, https://doi.org/10.1007/3-540-37689-5.

[24] R. Herzog and C. Meyer, *Optimal control of static plasticity with linear kinematic hardening*, ZAMM J. Appl. Math. Mech., 91 (2011), pp. 777–794.

[25] R. Herzog, C. Meyer, and G. Wachsmuth, *Integrability of displacement and stresses in linear and nonlinear elasticity with mixed boundary conditions*, J. Math. Anal. Appl., 382 (2011), pp. 802–813.

[26] R. Herzog, C. Meyer, and G. Wachsmuth, *C-stationarity for optimal control of static plasticity with linear kinematic hardening*, SIAM J. Control Optim., 50 (2012), pp. 3052–3082, https://doi.org/10.1137/100809325.

[27] R. Herzog, C. Meyer, and G. Wachsmuth, *B- and strong stationarity for optimal control of static plasticity with hardening*, SIAM J. Optim., 23 (2013), pp. 321–352, https://doi.org/10.1137/110821147.

[28] R. Herzog, C. Meyer, and G. Wachsmuth, *Optimal control of elastoplastic processes: Analysis, algorithms, numerical analysis and applications*, in Trends in PDE Constrained Optimization, Springer, 2014, pp. 27–41.

[29] I. Hlaváček, *Shape optimization of elastoplastic bodies obeying Hencky's law*, Apl. Mat., 31 (1986), pp. 486–499.

[30] I. Hlaváček, *Shape optimization of an elasto-perfectly plastic body*, Apl. Mat., 32 (1987), pp. 381–400.

[31] I. Hlaváček, *Shape optimization of elasto-plastic axisymmetric bodies*, Appl. Math., 36 (1991), pp. 469–491.

[32] S. Kaliszky, J. Logo, and T. Havady, *Optimal design of elasto-plastic structures under various loading conditions and displacement constraints*, Period. Polytech. Civil Engrg., 33 (1989), pp. 107–122.

[33] R. Karkauskas, *Optimization of elastic-plastic geometrically non-linear lightweight structures under stiffness and stability constraints*, J. Civil Engrg. Manag., 10 (2004), pp. 97–106.

[34] J. Kato, H. Hoshiba, S. Takase, K. Terada, and T. Kyoya, *Analytical sensitivity in topology optimization for elastoplastic composites*, Struct. Multidiscip. Optim., 52 (2015), pp. 507–526.

[35] M. Khanzadi and S. M. Tavakkoli, *Optimal plastic design of frames using evolutionary structural optimization*, Int. J. Civil Engrg., 9 (2011), pp. 175–170.

[36] A. Khludnev, *Optimal control in one-dimensional elastic-plastic models*, J. Appl. Mech. Tech. Phys., 32 (1991), pp. 760–763.

[37] N. H. Kim, K. K. Choi, and J. Chen, *Shape design sensitivity analysis and optimization of elasto-plasticity with frictional contact*, AIAA J., 38 (2000), pp. 1742–1753.

[38] N. H. Kim, K. K. Choi, and J. S. Chen, *Structural optimization of finite deformation elasto-plasticity using continuum-based shape design sensitivity formulation*, Comput. Structures, 79 (2001), pp. 1959–1976.

[39] M. Kocvara and J. V. Outrata, *Shape optimization of elasto-plastic bodies governed by variational inequalities*, in Boundary Control and Variation, Lecture Notes in Pure Appl. Math. 163, Marcel Dekker, 1994, pp. 261–271.

[40] T. Lee, J. Arora, and V. Kumar, *Shape design sensitivity analysis of viscoplastic structures*, Comput. Methods Appl. Mech. Engrg., 108 (1993), pp. 237–259.

[41] D. Löbach, *Interior stress regularity for the Prandtl Reuss and Hencky model of perfect plasticity using the Perzyna approximation*, no. 386 in Bonner Math. Schriften, Rheinische Friedrich-Wilhelms-Universität, Mathematisches Institut, 2007.

[42] A. Maury, *Shape Optimization for Contact and Plasticity Problems Thanks to the Level Set Method*, Ph.D. thesis, Université Pierre et Marie Curie–Paris VI, 2016, https://tel.archives-ouvertes.fr/tel-01442801.

[43] K. Maute, S. Schwarz, and E. Ramm, *Adaptive topology optimization of elastoplastic structures*, Struct. Optim., 15 (1998), pp. 81–91.

[44] P. Michaleris, D. A. Tortorelli, and C. A. Vidal, *Tangent operators and design sensitivity formulations for transient non-linear coupled problems with applications to elastoplasticity*, Int. J. Numer. Methods Engrg., 37 (1994), pp. 2471–2499.

[45] J. J. Moreau, *Evolution problem associated with a moving convex set in a Hilbert space*, J. Differential Equations, 26 (1977), pp. 347–374, https://doi.org/10.1016/0022-0396(77)90085-7.

[46] J. J. Moreau and P. D. Panagiotopoulos, eds., *Nonsmooth Mechanics and Applications*, CISM International Centre for Mechanical Sciences 302, Springer, 2014.

[47] F. Murat and J. Simon, *Etudes de problèmes d'optimal design*, Lecture Notes in Comput. Sci. 41, Springer-Verlag, 1976, pp. 54–62.

[48] S. Osher and R. Fedkiw, *Level Set Methods and Dynamic Implicit Surfaces*, Appl. Math. Sci. 153, Springer-Verlag, New York, 2003.

[49] S. Osher and J. Sethian, *Front propagating with curvature dependent speed: Algorithms based on Hamilton-Jacobi formulations*, J. Comput. Phys., 78 (1988), pp. 12–49.

[50] C. B. Pedersen, *Topology optimization of 2D-frame structures with path-dependent response*, Int. J. Numer. Methods Engrg., 57 (2003), pp. 1471–1501.

[51] O. Pironneau, *Optimal Shape Design for Elliptic Systems*, Springer Ser. Comput. Phys., Springer-Verlag, New York, 1984, https://doi.org/10.1007/978-3-642-87722-3.

[52] V. Pištora, *Shape optimization of an elasto-plastic body for the model with strain-hardening*, Apl. Mat., 35 (1990), pp. 373–404.

[53] R. Rannacher and F.-T. Suttmeier, *A posteriori error estimation and mesh adaptation for finite element models in elasto-plasticity*, Comput. Methods Appl. Mech. Engrg., 176 (1999), pp. 333–361.

[54] E. Rohan and J. Whiteman, *Shape optimization of elasto-plastic structures and continua*, Comput. Methods Appl. Mech. Engrg., 187 (2000), pp. 261–288.

[55] T. Roubíček, *Nonlinear Partial Differential Equations with Applications*, Int. Ser. Numer. Math. 153, Birkhäuser, 2013.

[56] M. Sauter, *Numerical Analysis of Algorithms for Infinitesimal Associated and Non-associated Elasto-plasticity*, Ph.D. thesis, Karlsruhe Inst. für Technologie, Karlsruhe, Germany, 2010.

[57] S. Schwarz, K. Maute, and E. Ramm, *Topology and shape optimization for elastoplastic structural response*, Comput. Methods Appl. Mech. Engrg., 190 (2001), pp. 2135–2155.

[58] Scilab Enterprises, *Scilab: Le logiciel open source de calcul numérique*, Scilab Enterprises, 2012, http://www.scilab.org.

[59] J. Sethian, *Level Set Methods and Fast Marching Methods, Evolving Interfaces in Computational Geometry, Fluid Mechanics, Computer Vision, and Materials Science*, 2nd ed., Cambridge Monogr. Appl. Comput. Math. 3, Cambridge University Press, 1999.

[60] J. C. Simo and T. J. Hughes, *Computational Inelasticity*, Interdiscip. Appl. Math. 7, Springer-Verlag, 2006.

[61] J. Simon, *Differentiation with respect to the domain in boundary value problems*, Numer. Funct. Anal. Optim., 2 (1980), pp. 649–687.

[62] J. Sokolowski and J.-P. Zolesio, *Introduction to Shape Optimization. Shape Sensitivity Analysis*, Springer Ser. Comput. Math. 16, Springer-Verlag, Berlin, 1992, https://doi.org/10.1007/978-3-642-58106-9.

[63] P. M. Suquet, *Un espace fonctionnel pour les équations de la plasticité*, Ann. Fac. Sci. Toulouse Math., 1 (1979), pp. 77–87.

[64] P. M. Suquet, *Sur les équations de la plasticité: Existence et régularité des solutions*, J. Mécanique, 20 (1981), pp. 3–39.

[65] C. Talischi, G. H. Paulino, A. Pereira, and I. F. Menezes, *Polygonal finite elements for topology optimization: A unifying paradigm*, Int. J. Numer. Methods Engrg., 82 (2010), pp. 671–698.

[66] L. Tao and D. Zichen, *Design optimization for truss structures under elasto-plastic loading condition*, Acta Mech. Solida Sin., 19 (2006), pp. 264–274.

[67] R. Temam, *Problèmes mathématiques en plasticité*, Math. Methods Inform. Sci. 12, Gauthier-Villars, 1983.

[68] C. A. Vidal and R. B. Haber, *Design sensitivity analysis for rate-independent elastoplasticity*, Comput. Methods Appl. Mech. Engrg., 107 (1993), pp. 393–431.

[69] G. Wachsmuth, *Optimal control of quasi-static plasticity with linear kinematic hardening, part* I*: Existence and discretization in time*, SIAM J. Control Optim., 50 (2012), pp. 2836–2861, https://doi.org/10.1137/110839187.

[70] M. Y. Wang, X. Wang, and D. Guo, *A level set method for structural topology optimization*, Comput. Methods Appl. Mech. Engrg., 192 (2003), pp. 227–246.

[71] K. Washizu, *Variational Methods in Elasticity and Plasticity*, Elsevier Science & Technology, 1974, https://books.google.fr/books?id=jpseAQAAIAAJ.

[72] C. Wieners, *Orthogonal Projections onto Convex Sets and the Application to Problems in Plasticity*, preprint, 1999.

[73] C. Wieners, *Nonlinear solution methods for infinitesimal perfect plasticity*, ZAMM J. Appl. Math. Mech., 87 (2007), pp. 643–660.

[74] K. Yuge and N. Kikuchi, *Optimization of a frame structure subjected to a plastic deformation*, Struct. Optim., 10 (1995), pp. 197–208.

[75] E. H. Zarantonello, *Projections on convex sets in Hilbert space and spectral theory. Part* I*. Projections on convex sets: Part* II*. Spectral theory*, in Contributions to Nonlinear Functional Analysis, Proceedings of a Symposium Conducted by the Mathematics Research Center, University of Wisconsin–Madison, 1971, pp. 237–424.